JOURNAL OF THE MECHANICAL BEHAVIOR OF BIOMEDICAL MATERIALS 37 (2014) 141–152

Available online at www.sciencedirect.com

ScienceDirect

www.elsevier.com/locate/jmbbm

Research Paper

Multiscale characterization of acrylic bone cement modified with functionalized mesoporous silica nanoparticles

Josh Slane[a,c,*], Juan Vivanco[b,e], Donna Ebenstein[d], Matthew Squire[c], Heidi-Lynn Ploeg[a,b]

[a]Materials Science Program, University of Wisconsin-Madison, Madison, WI, USA
[b]Department of Mechanical Engineering, University of Wisconsin-Madison, Madison, WI, USA
[c]Department of Orthopedics and Rehabilitation, University of Wisconsin-Madison, Madison, WI, USA
[d]Department of Biomedical Engineering, Bucknell University, Lewisburg, PA, USA
[e]Facultad de Ingeniería y Ciencias, Universidad Adolfo Ibañez, Viña del Mar, Chile

ARTICLE INFO

Article history:
Received 22 April 2014
Accepted 15 May 2014
Available online 24 May 2014

Keywords:
Bone cement
Mechanical properties
Nanoindentation
Reinforced polymer
Orthopedics

ABSTRACT

Acrylic bone cement is widely used to anchor orthopedic implants to bone and mechanical failure of the cement mantle surrounding an implant can contribute to aseptic loosening. In an effort to enhance the mechanical properties of bone cement, a variety of nanoparticles and fibers can be incorporated into the cement matrix. Mesoporous silica nanoparticles (MSNs) are a class of particles that display high potential for use as reinforcement within bone cement. Therefore, the purpose of this study was to quantify the impact of modifying an acrylic cement with various low-loadings of mesoporous silica. Three types of MSNs (one plain variety and two modified with functional groups) at two loading ratios (0.1 and 0.2 wt/wt) were incorporated into a commercially available bone cement. The mechanical properties were characterized using four-point bending, microindentation and nanoindentation (static, stress relaxation, and creep) while material properties were assessed through dynamic mechanical analysis, differential scanning calorimetry, thermogravimetric analysis, FTIR spectroscopy, and scanning electron microscopy. Four-point flexural testing and nanoindentation revealed minimal impact on the properties of the cements, except for several changes in the nano-level static mechanical properties. Conversely, microindentation testing demonstrated that the addition of MSNs significantly increased the microhardness. The stress relaxation and creep properties of the cements measured with nanoindentation displayed no effect resulting from the addition of MSNs. The measured material properties were consistent among all cements. Analysis of scanning electron micrographs images revealed that surface functionalization enhanced

*Coreespondence to: Materials Science Program, University of Wisconsin-Madison, 1513 University Ave, Room 3046, Madison, WI, 53706, USA. Tel.: +1 608 263 6692; fax: +1 608 2652316.
E-mail address: jaslane@wisc.edu (J. Slane).

http://dx.doi.org/10.1016/j.jmbbm.2014.05.015
1751-6161/

particle dispersion within the cement matrix and resulted in fewer particle agglomerates. These results suggest that the loading ratios of mesoporous silica used in this study were not an effective reinforcement material. Future work should be conducted to determine the impact of higher MSN loading ratios and alternative functional groups.

1. Introduction

Proper implant fixation is vital to ensure the long-term success of an orthopedic implant. Two primary methods are used to achieve fixation: press-fit/biological fixation where bone growth onto the implant's surface provides anchorage or with acrylic bone cement that acts as a grouting material between the implant and bone (Jayasuriya et al., 2013; Khanuja et al., 2011). With respect to data obtained from long-term joint registry databases, the use of bone cement is considered the 'gold standard' of implant fixation (Hailer et al., 2010). Despite this, aseptic loosening remains the primary cause of revision arthroplasty regardless of the chosen fixation technique (Adelani et al., 2013; Sonntag et al., 2012). One of the leading factors contributing to the development of aseptic loosening is mechanical failure of the cement mantle (Jeffers et al., 2007), which can occur at one or more of the three 'weak zones': the cement-implant interface, within the cement mantle itself or the cement-bone interface (Lewis, 2003).

In an effort to enhance the static and dynamic mechanical properties of bone cement, reinforcement materials can be incorporated within the powder or monomer component prior to mixing. A wide variety of materials have been investigated such as carbon nanotubes (Marrs et al., 2006; Ormsby et al., 2010b, 2012), titanium oxide fibers (Khaled et al., 2011), zirconia fibers (Kane et al., 2010), and polyethylene terephthalate fibers (Kumar and Cooke, 2006), along with others. Issues regarding interfacial adhesion, high stiffness and poor handling characteristics have generally prevented these composite cements from transitioning from the bench top to clinical practice, despite several encouraging in vitro results (Lennon, 2008).

Mesoporous silica nanoparticles (MSNs) show high potential for use as a polymer reinforcement due to their small particle size, large surface area, high pore volume and homogeneous structure (Izquierdo-Barba et al., 2008; Zhang et al., 2010). The high surface area of MSNs indicates that small loading ratios can be used to provide significant mechanical reinforcement, similar to that observed with carbon nanotubes (Ormsby et al., 2010a). Additionally, the spherical nature of MSNs offers an advantage over other reinforcement materials such as carbon nanotubes, which are often difficult to disperse due to strong Van der Waals forces and physical entanglements (Pegel et al., 2008), which can severely limit their usefulness (Ania et al., 2006). Silica/polymer nanocomposites have been shown to possess superior mechanical properties relative to neat polymers (Ji et al., 2003; Lach et al., 2006), however, the weight percentage ratios typically employed are high (10–20% wt/wt). While this is acceptable for industrial applications that can utilize specialized homogenization and mixing techniques, high particle-loading ratios are difficult to disperse within bone cement since the cement must be prepared immediately at the time of surgery. It is important therefore that the addition of particles does not alter the mixing and handling characteristics of cement, otherwise the clinical usefulness may be compromised.

A wide variety of testing methods spanning multiple length scales can be used to characterize particle-reinforced polymers. Indentation techniques, such as micro and nanoindentation, can provide details on reinforcement mechanisms since they operate at small force/displacement scales allowing for individual components to be analyzed which may thus otherwise be difficult to quantity with traditional bulk testing methods (Beake et al., 2002; Dhakal et al., 2006). With respect to acrylic cements, microindentation has been used to examine the change in mechanical properties resulting from the addition of antibiotics (Musib et al., 2012), particulate-fillers (Chung et al., 2005), and silica-fused whiskers (Xu et al., 2002) and changes induced following implantation in patients (Chaplin et al., 2006). Similarly, nanoindentation has been used to characterize the fracture properties (Ayatollahi and Karimzadeh, 2012), elastic modulus, and hardness (Karimzadeh and Ayatollahi, 2012) of acrylic bone cement. Additionally, Arun et al. used nanoindentation to evaluate the mechanical properties of bone cement modified with functionalized single-walled carbon nanotubes and determined the optimal loading ratio for peak modulus and hardness to be 0.15% wt/wt (Arun et al., 2014).

Previously, we reported on the static and fatigue properties of acrylic bone cement modified with various loadings of MSNs (0.5, 2 and 5% wt/wt) and found a general decrease in several mechanical properties with increasing MSN content (Slane et al., 2014). These results were attributed to inadequate dispersion and poor interfacial adhesion between the particle and polymer matrix, compounded by the relatively high loading ratios used. A potential method to overcome these shortcomings is to use surface modified nanoparticles, where various functional groups are linked to the particle surface. Surface functionalization can act to stabilize nanoparticles while enhancing their dispersion and compatibility with the polymer matrix (Guo et al., 2006; Kordás et al., 2013). Therefore, the aim of the current study was to investigate the influence of low-loadings of surface-modified mesoporous silica on the mechanical and material properties of acrylic bone cement. A commercially available acrylic bone cement was modified with several different loading ratios of unmodified MSNs (as a control) and two types of surface functionalized MSNs. A multiscale approach was used to characterize the cement's mechanical properties and the macro,

micro and nano-level properties were quantified. Additionally, the effects of MSN inclusion and surface functionalization on the dynamic, thermal and material properties of the cements were assessed.

2. Materials and methods

2.1. Cement preparation

A commercially available bone cement was used in this study (Palacos R, Heraeus Medical GmbH, Wehrheim, Germany). The powder component contained of 33.6 g poly(methyl methacrylate), 0.3 g benzoyl peroxide, 6.1 g zirconium dioxide (a radiopacifier), and scant chlorophyll while the liquid monomer contained 18.4 g methyl methacrylate ($\leq$30 ppm hydroquinone used as an inhibitor) and 0.4 g N,N-dimethyl-p-toluidine. For all testing, a 2:1 powder-to-monomer ratio was used.

Mesoporous silica nanoparticles, with an average particle diameter of 200 nm, were obtained from a chemical supply company (Sigma Aldrich, St. Louis, MO, USA). Three types of MSNs were used in loading ratios of 0.1 and 0.2 wt/wt relative to the powder: plain unmodified (SiO_2), propylamine functionalized (NH_2) and propylcarboxylic acid functionalized (COOH). MSNs had a surface area of 720 m^2/g, average pore diameter of 4.5 nm, and a total pore volume of 0.82 cm^3/g, as determined with nitrogen adsorption (Autosorb-1, Quantachrome, Boynton Beach, FL, USA). In total, there were six experimental groups containing MSNs (three particle types, two loading ratios) and the plain cement was a control.

MSNs were dispersed within the liquid monomer using an ultrasonic homogenizer (150VT, Biologics Inc, Manassas, VA, USA) with a mixing time of 3 min. The monomer/MSN mixture was sonicated within a jacketed reaction vessel with cold water continuously circulated through the vessel. Additionally, the homogenizer was operated in a pulsed power mode to mitigate monomer heating. For the configured mixing setup, the delivered acoustic power was calculated to be 15 W, which was determined using the calorimetric method (Taurozzi et al., 2011). In an effort to coax the monomer to flow into the pores of the MSNs and degas any entrapped air, the mixture was immediately transferred to a vacuum chamber following sonication and subjected to a vacuum pressure of $-$800 mbar for 3 min. To ensure consistency among all samples, the control cement was prepared using the same technique.

The monomer and powder were combined by hand in a polymer mixing bowl for 30 s, spaulated into aluminum molds, and allowed to cure for 30 min. Although not measured, on a qualitative level the handling characteristics of the cements were not altered by the addition of MSNs. Following removal from the mold, samples were wet ground with 400 grit silicon carbide paper. To ensure complete curing, samples were stored for one week at ambient conditions (21 °C, 22% humidity) prior to performing any testing. Samples for microindenation and nanoindentation were embedded in epoxy, ground with silicon carbide paper (240, 400, 600, 800, and 1200 grit), and polished to a uniform surface roughness with polycrystalline diamond suspensions (6, 1, and 0.25 μm).

2.2. Mechanical testing

2.2.1. Macro level

An electromechanical materials testing frame equipped with a 250 N load cell was used to conduct all static testing (Criterion C43.104, MTS Systems, Eden Prairie, MN, USA). Force and displacement data were collected at 100 Hz. Four-point flexural tests were conducted at a displacement rate of 5 mm/min using an outer span of 60 mm and an inner span of 20 mm. Testing was conducted until failure using flat beam samples with a length, width and, thickness 75 ± 0.01, 9.96 ± 0.01 and 3.30 ± 0.02 mm, respectively. A minimum of seven samples per experimental group were tested. Flexural modulus, E, was determined using Eq. 1 (Malzbender and Steinbrech, 2004):

$$E = \frac{a(3Lx-3x^2-a^2)}{12I}\frac{\Delta F}{\Delta d} \quad (1)$$

where a is the distance between inner supports, L is the distance between outer supports, x the position at which deflection is measured, I the area moment of inertia, and $\Delta F/\Delta d$ the slope of the linear portion of the force–displacement curve. In this study, specimen displacement was measured at the point of load application (i.e. $x=a$). Flexural strength, σ_F, was determined from:

$$\sigma_F = \frac{3Fa}{bh^2} \quad (2)$$

where F is the applied load at failure, b the sample width, and h the sample thickness.

2.2.2. Microindentation

Microindentation testing was conducted using a commercially available indentation system (Tukon 1202, Buehler, Lake Bluff, IL, USA). A diamond-tipped Vickers indenter was used to apply a peak load of 9.8 N with a dwell time of 10 s. For each cement group, two samples were tested with 10 indents performed per sample (i.e. 20 indents per cement group). The diagonals of the residual indent were immediately measured with the internal optics of the system. Indents were placed a minimum of three diagonals apart to ensure no interaction. Hardness, H, was calculated using:

$$H = \left(1.854\cdot\frac{F}{d^2}\right)\cdot 9.807 \quad (3)$$

where F is the applied indentation load and d the average diagonal of the indent. Collected hardness data were further analyzed with the linearized two-parameter Weibull distribution (Padmanabhan et al., 2010):

$$\ln\left[\ln\left(\frac{1}{1-P_i}\right)\right] = m\ln H - m\ln H_c \quad (4)$$

where m is the Weibull modulus (a measure of data scatter), H_c the scale parameter or characteristic hardness (where the probability of occurrence is 63.2%), and P_i the cumulative probability (Lewis and Janna, 2003).

2.2.3. Nanoindentation

A Hysitron TI 950 TriboIndenter (Hysitron Inc, Eden Prairie MN, USA) equipped with a diamond-tipped Berkovich probe was used to perform nanoindentation. Prior to the start of testing, the machine compliance was determined by performing a series of indents on a fused silica standard. Additionally, a probe calibration procedure was completed to ensure reliable contact area measurements. However, as indent depths were much greater than the maximum calibrated probe depth (~200 nm), the idealized Berkovich shape function ($A(h_c)=24.5h_c^2$) was utilized for modulus and hardness calculations All testing was conducted enclosed within the TriboIndenter's housing at ambient laboratory conditions (~23 °C). Static indentation testing was performed using a trapezoidal loading function with a peak displacement of 750 nm, a loading/unloading rate of 25 nm/s, and a dwell time of 15 s. Load and displacement data were recorded at 200 Hz. For each sample, a minimum of 38 indents were performed with a spacing of 250 μm between each indent. The obtained load–displacement data were analyzed with the Oliver–Pharr method (Oliver and Pharr, 2004). Additionally, the plasticity index, ψ, of the cements was calculated from:

$$\psi = \frac{h_{max} - h_f}{h_{max}} \tag{5}$$

where h_{max} is the maximum penetration depth during loading and h_f the final unloading depth. The plasticity index varies from 0 to 1, where 0 represents fully-elastic behavior and 1 represents fully plastic material behavior (Karimzadeh and Ayatollahi, 2012).

The time-dependent properties of the cements were determined using stress relaxation and creep tests. For stress relaxation, a minimum of 18 indents were performed per sample. The same parameters and loading profile as used in static testing were utilized with the exception that the dwell time was increased to 60 s. The relaxation modulus, $G(t)$, was determined from (Schiffmann, 2006):

$$G(t) = 2(1-\upsilon^2)\tan\beta\left(\frac{P(t)}{A}\right) \tag{6}$$

where υ is Poisson's ratio (0.3), β the half angle of indenter tip (65.35°), $P(t)$ the applied load at any time t, and A the contact area determined from the Berkovich shape function. In a stress relaxation test, the contact area is constant since the indentation depth does not change throughout the test. It is important to note that during nanoindentation, sample deformation is not pure shear but rather a complex state of multi-axial compression and shear. Despite this, the relationship between stress and strain should be independent of the deformation mechanism (Schiffmann, 2006).

Creep testing was performed with a trapezoidal loading function with a peak load of 2500 μN, a loading/unloading rate of 250 μN/s, and a dwell time of 100 s. A minimum of six indents were performed per sample. The creep behavior of the cements were modeled using a combined Maxwell–Voigt four element model (also known as a burger model) (Fischer-Cripps, 2011):

$$h^2(t) = \frac{\pi}{2}P_o\cot\alpha\left[\frac{1}{E_1}+\frac{1}{E_2}\left(1-e^{-t\frac{E_2}{c}}\right)+\frac{1}{\eta}t\right] \tag{7}$$

where h is the penetration depth as a function of time, t, P_o the applied load, α the equivalent cone angle of the Berkovich tip (70.3°), E_1 and E_2 the moduli (GPa), η the long-term creep viscosity (GPa s), and c/E_2 the creep time constant (s). Values of E_1, E_2, η, and c were estimated by performing nonlinear least-squares curve fitting of the experimentally obtained deformation (indenter penetration) data to Eq. (7) (MATLAB, Mathworks, Natick, MA).

2.3. Material characterization

2.3.1. Morphology

The microstructural morphology of the failure surface of four-point bending samples was investigated with scanning electron microscopy (SEM). Samples were mounted on aluminum stubs and sputter coated with gold for 30 s. Images were then obtained with a LEO DSM 1530 field emission SEM (Zeiss-LEO, Oberkochen, Germany) using an acceleration voltage of 5 kV and working distance of 5 mm.

2.3.2. Dynamic properties

Dynamic mechanical analysis (DMA) was used to assess the viscoelastic properties of the cements. Flat beam samples (3 mm thickness, 9.92 mm width) were subjected to dynamic strain sweeps from 0.005% to 0.08% at 37 °C using a three-point bending configuration with a 40 mm span (RSA III, TA Instruments, New Castle, DE, USA). Loading frequencies of 1, 10 and 40 Hz were used and a constant static force of 0.085 N was applied to the samples to ensure continuous contact with the bending fixture throughout testing. The higher loading frequencies used (10 and 40 Hz) approach the range of traumatic impact loading (Park et al., 2004) while the strain levels are within the range seen within the cement mantle surrounding a femoral prosthesis during the single-limb stance phase of gait (O'Connor et al., 1996).

2.3.3. Chemical analysis

Structural changes in the cement caused by the inclusion of MSNs were monitored with Fourier transform infrared spectroscopy (Equinox 55, Bruker, Billerica, MA, USA) between 4000 and 750 cm^{-1} at a resolution of 2 cm^{-1}. Cement cross sections were scanned in attenuated total reflectance (ATR) mode at three random sections on each sample, with 32 scans taken at each location. All collected spectra were averaged to obtain one representative spectra per cement.

2.3.4. Thermal characteristics

The thermal degradation properties of the cement composites were investigated using thermogravimetric analysis (Q500, TA Instruments, New Castle, DE, USA). Thermograms were obtained from 30 to 600 °C in a nitrogen environment using a linear heating rate of 20 °C/min. The initial thermal decomposition temperature, T_{10}, was taken as the point where 10% of the material had decomposed while the mid-point decomposition, T_{50}, the point where 50% of the material had decomposed.

The glass transition temperatures, T_g, of the cements were determined using a differential scanning calorimeter (Q100, TA Instruments, New Castle, DE, USA). Samples between 4 and 6 mg were sealed in aluminum pans and subjected to

heating/cooling/heating cycles between 10 and 160 °C at 10 °C/min. The T_g was determined from the second heating cycle using the method described in ASTM D3418 (ASTM International, 2012).

2.4. Statistics

Statistical analysis was conducted with commercially available software (Minitab Inc, State College, PA, USA) and the significance level was set at 0.05 for all observations. Micro and nanoindentation data were found to exhibit non-normal distributions using the Anderson–Darling test, therefore, non-parametric analyses were employed. These data were evaluated with the Kruskal–Wallis test and the Mann–Whitney *U*-test with Bonferroni correction was used for post-hoc analysis. All other collected data were processed using analysis of variance (ANOVA) with Tukey's HSD post-hoc analysis. Where appropriate, data are presented as mean ± standard deviation.

3. Results

3.1. Mechanical testing

3.1.1. Macro level

ISO 5833 (International Organization for Standardization, 2002) establishes benchmark values for the flexural properties of acrylic bone cement of 50 MPa and 1.8 GPa for the flexural strength and modulus, respectively. All cements tested in this study vastly exceed these requirements. It should be noted that samples in this study were cured for one week following fabrication, while in the ISO standard it calls for 24 h. While this increase in curing time can enhance the mechanical properties, the relative change from one to seven days is not drastic (Nottrott et al., 2007).

The inclusion of MSNs had no significant effect on either the flexural modulus or flexural strength relative to standard Palacos bone cement (Table 1). Additionally, results were consistent across all MSN groups indicating there was no significant effect resulting from surface functionalization. The flexural properties slightly decreased with the addition of nanoparticles, however, these changes were minimal with a peak percent difference of 4.4% for modulus and 3.0% for strength.

Table 1 – Results (mean ± SD) obtained from static mechanical testing. E_f – flexural modulus and σ_f – flexural strength.

Sample	E_f (GPa)	σ_f (MPa)
Palacos	2.81 ± 0.09	72.07 ± 3.38
0.1% SiO_2	2.78 ± 0.06	70.53 ± 2.91
0.2% SiO_2	2.77 ± 0.08	69.93 ± 3.99
0.1% NH_2	2.77 ± 0.04	72.01 ± 1.67
0.2% NH_2	2.71 ± 0.07	70.38 ± 2.57
0.1% COOH	2.69 ± 0.05	70.61 ± 2.17
0.2% COOH	2.79 ± 0.02	70.01 ± 3.67

3.1.2. Microindentation

The addition of mesoporous silica particles, regardless of surface treatment or loading ratio, significantly increased microindentation hardness (Table 2). Relative to standard Palacos, the addition of MSNs increased microhardness by 3.7–8.6%. For 0.1% MSN loading ratios, surface functionalization significantly affected hardness with $SiO_2 < NH_2 <$ COOH. Interestingly, the same finding was not observed for 0.2% loadings. No significant difference was found between 0.2% SiO_2 and 0.2% NH_2, however, the hardness of 0.2% COOH was significantly lower than both. Additionally, it was found that increasing the MSN content from 0.1% to 0.2% significantly increased hardness for SiO_2 and NH_2 groups, but not COOH.

Weibull plots for the collected hardness data are shown in Fig. 1 and values for the Weibull modulus and characteristic strength are given in Table 2. The estimated Weibull moduli were generally high, with the lowest record value being for cement containing 0.2% COOH. With increasing MSN content, the Weibull modulus tended to decrease. The characteristic strength increased with the addition of MSNs.

3.1.3. Nanoindentation

Results from static nanoindentation testing are given in Table 3. Relative to Palacos only one cement, regardless of particle loading ratio and surface functionalization, displayed a significantly different modulus, 0.1% COOH (a 4.4% increase).

Table 2 – Results (mean ± SD) obtained from microindentation testing. H – hardness, m – Weibull modulus, H_C – characteristic hardness.

Sample	H (MPa)	m	H_C (MPa)
Palacos	172.8 ± 3.2	62.1	174.3
0.1% SiO_2	179.2 ± 1.7[a]	117.9	180.1
0.2% SiO_2	187.7 ± 2.5[a]	81.1	188.9
0.1% NH_2	182.6 ± 1.9[a]	108.8	183.5
0.2% NH_2	186.6 ± 2.3[a]	92.1	187.7
0.1% COOH	185.4 ± 3.7[a]	57.6	187.2
0.2% COOH	182.6 ± 3.7[a]	32.5	180.8

[a] $p < 0.001$, relative to Palacos.

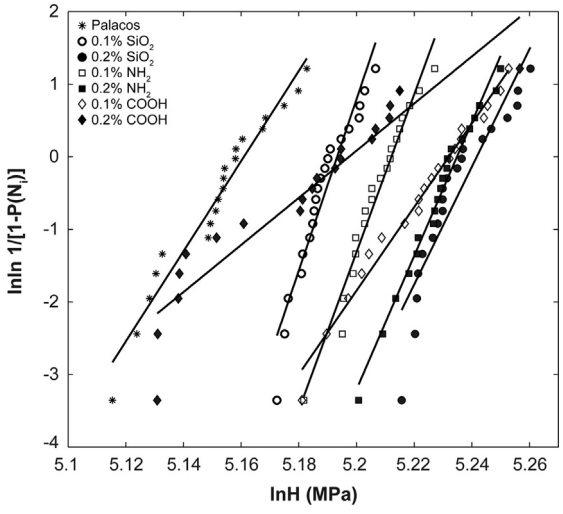

Fig. 1 – Weibull plots for the measured hardness data.

Table 3 – Results (mean ± SD) obtained from nanoindentation testing. E_s – modulus, H – hardness, ψ – plasticity index, and relaxation modulus $G(t)$ evaluated at 1 and 10 s.

Sample	E_s (GPa)	H (MPa)	ψ	G (t=1 s) (GPa)	G (t=10 s) (GPa)
Palacos	3.83 ± 0.24	195.7 ± 31.3	0.376 ± 0.064	0.87 ± 0.09	0.73 ± 0.09
0.1% SiO_2	3.96 ± 0.26	207.4 ± 30.6	0.398 ± 0.047	0.89 ± 0.09	0.75 ± 0.09
0.2% SiO_2	3.69 ± 0.37	179.2 ± 23.4[a]	0.329 ± 0.070[a]	0.84 ± 0.11	0.70 ± 0.10
0.1% NH_2	3.86 ± 0.24	203.2 ± 31.8	0.388 ± 0.057	0.90 ± 0.11	0.76 ± 0.11
0.2% NH_2	3.92 ± 0.14	217.8 ± 34.7[a]	0.378 ± 0.033	0.94 ± 0.11	0.79 ± 0.11
0.1% COOH	4.00 ± 0.21[a]	217.0 ± 22.9[a]	0.367 ± 0.033	0.90 ± 0.09	0.78 ± 0.10
0.2% COOH	3.81 ± 0.27	203.2 ± 32.8	0.374 ± 0.061	0.87 ± 0.10	0.73 ± 0.10

[a] $p < 0.05$, relative to Palacos.

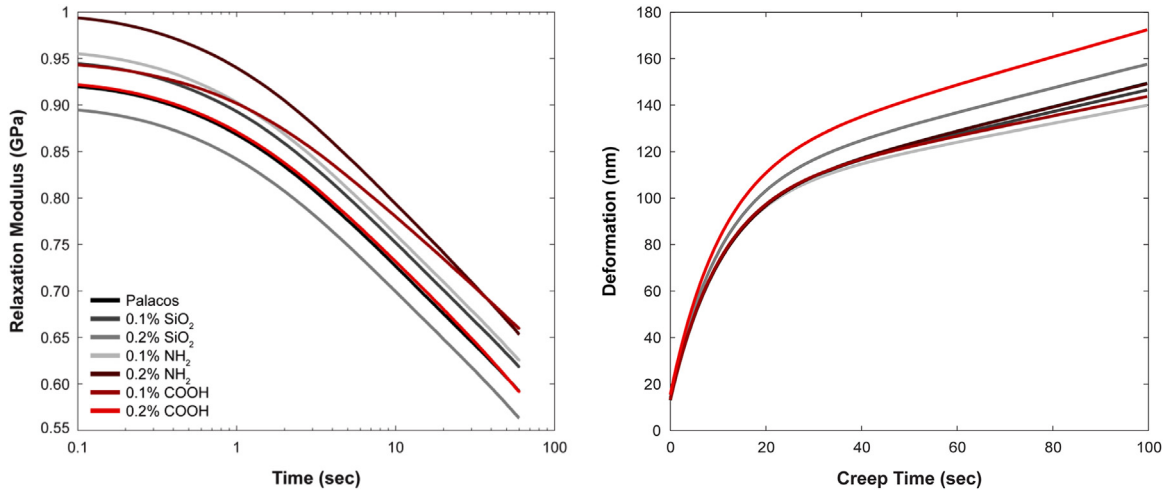

Fig. 2 – Plots of the calculated relaxation moduli, $G(t)$ (left). Plots of the burger model fit for each cement. For clarity, only the curve fit of the burger model is shown, and not the experimental data (right). The same legend applies to both figures.

Table 4 – The estimated parameters (mean ± SD) of the burger model fit to the collected creep data. E_1 and E_2 are moduli and n is the long-term creep viscosity.

Cement	E_1 (GPa)	E_2 (GPa)	n (10^3 GPa s)	Creep Constant (s)
Palacos	123.2 ± 9.3	18.8 ± 1.5	3.2 ± 0.5	10.1 ± 0.1
0.1% SiO_2	121.7 ± 13.0	18.7 ± 2.1	3.5 ± 0.8	10.1 ± 0.3
0.2% SiO_2	115.3 ± 17.0	17.6 ± 2.4	3.2 ± 0.6	10.3 ± 0.5
0.1% NH_2	123.9 ± 13.7	18.4 ± 2.1	4.9 ± 2.8	10.2 ± 0.4
0.2% NH_2	124.0 ± 16.5	18.9 ± 2.2	3.2 ± 0.5	10.1 ± 0.3
0.1% COOH	120.6 ± 13.2	18.3 ± 2.1	4.1 ± 1.6	10.3 ± 0.3
0.2% COOH	105.2 ± 16.5	16.5 ± 2.4	2.8 ± 0.6	10.5 ± 0.4

For cements containing 0.2% loading ratios, modulus was significantly influenced by surface functionalization with NH_2 and COOH cements displaying higher moduli than SiO_2. The same trend was not observed for 0.1% loading ratios. Hardness was found to significantly decrease for 0.2% SiO_2 and increase for 0.1% COOH and 0.2% NH_2, relative to Palacos. Plasticity index was found to be consistent with the only significant difference being 0.2% SiO_2.

No significant difference in relaxation moduli was found and the magnitude of $G(t)$ was generally consistent amongst all cements (Table 3). The profile of $G(t)$ vs. time changed drastically after one second of relaxation time and began to degrade at a faster rate, as seen in Fig. 2. All cements displayed a uniform profile in $G(t)$ vs. time, except for 0.1% COOH, which interestingly had the lowest record modulus in static testing. No significant differences were observed in the creep behavior of the cements (Fig. 2). The collected data were well described by the burger model (adjusted R^2 of at least 0.995 for all cements), however, there were no significant differences in the estimated parameters (Table 4).

3.2. *Material characterization*

3.2.1. *Morphology*

Scanning electron micrographs revealed no apparent difference in the fracture surface of the cements (Fig. 3). Small pores between 50 and 100 μm were observed on the fracture surfaces of all cements and were not influenced by MSN

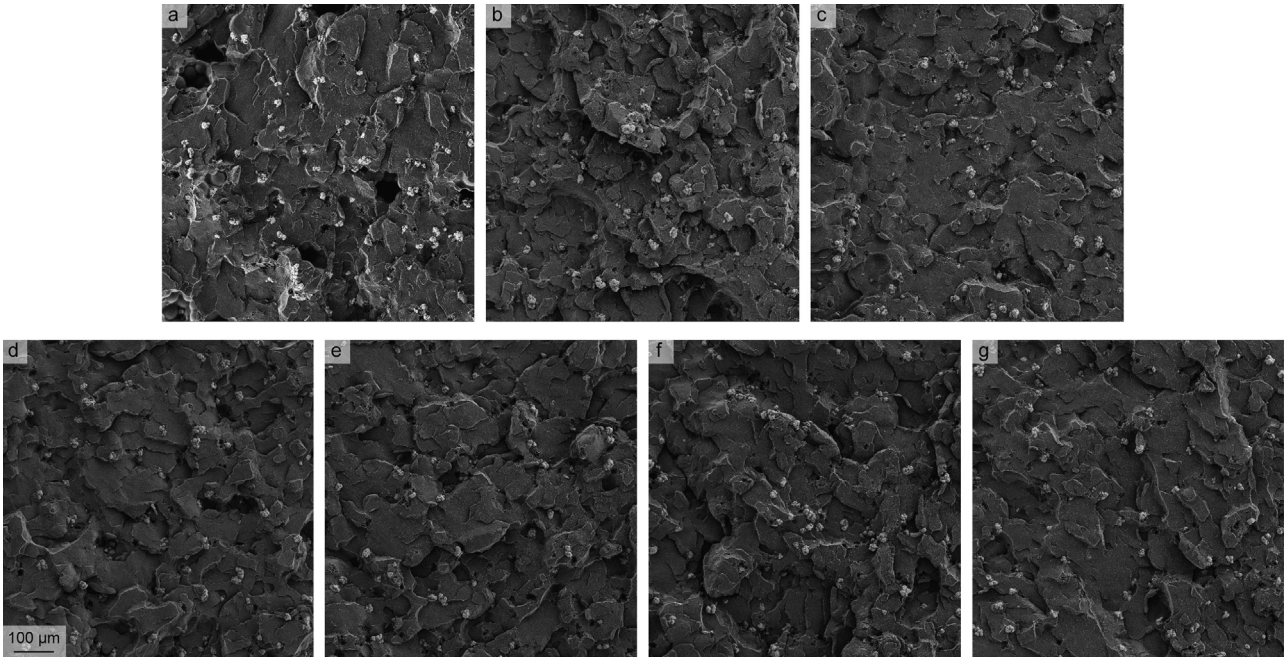

Fig. 3 – SEM images at 250×, taken from failure surface of four-point flexural samples. The scale bar applies to all images. (a) Palacos, (b) 0.1% SiO_2, (c) 0.2% SiO_2, (d) 0.1% NH_2, (e) 0.2% NH_2, (f) 0.1% COOH, and (g) 0.2% COOH.

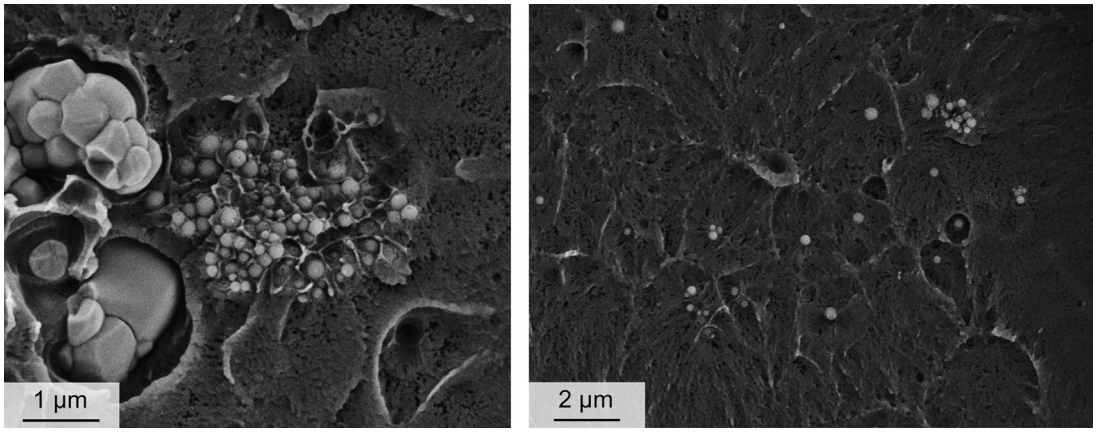

Fig. 4 – SEM images showing differences in MSN dispersion in the cement matrix. Left – SiO_2 particles at 20kx. Right – COOH particles at 15 kx.

inclusion or surface functionalization. The large cauliflower-like particles seen in the micrographs are zirconium dioxide, the radiopacifier material in the cement. Particle agglomerations were observed for all cements, however, the size of these agglomerations were considerably larger for SiO_2 particles (Fig. 4). Surface functionalization, both NH2 and COOH, was found to enhance the dispersion of MSNs within the cement matrix. Agglomerates were still observed for functionalized MSNs but they were smaller and occurred with less frequency than SiO_2 particles.

3.2.2. *Dynamic properties*

The storage modulus (E') and tan delta ($\tan\delta$) of the tested cements are shown in Fig. 5. All cements exhibited a linear viscoelastic range (where modulus is independent of applied strain, i.e. a flat response) from strain levels of approximately 0.0005–0.0015%. The storage modulus of all cements began to decrease sharply at a strain of 0.004%. For all loading frequencies cements displayed similar profiles and magnitudes in storage modulus and $\tan\delta$, indicating that the addition of MSNs had no substantial effect on the viscoelastic properties. The testing frequency was found to have a significant impact on the resulting viscoelastic properties, as expected. With increased frequency, the profile of storage modulus stayed consistent but the magnitude increased. Conversely, $\tan\delta$ displayed similar behavior in profile and magnitude for frequencies of 1 and 10 Hz, however, began to increase considerably at a strain of 0.005% for a loading frequency of 40 Hz.

3.2.3. *Chemical analysis*

Collected ATR-FTIR spectra displayed characteristic peaks for acrylic bone cement, as expected (Fig. 6). The most prominent

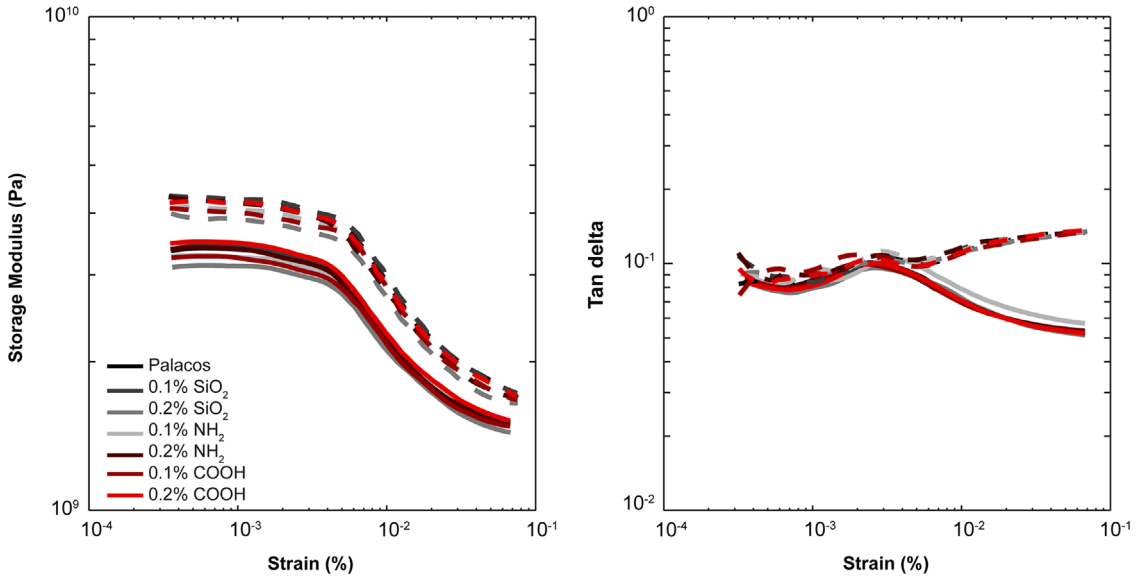

Fig. 5 – Results from DMA strain sweeps. Solid lines – 1 Hz, dashed lines – 40 Hz. For clarity purposes, data from 10 Hz is not shown.

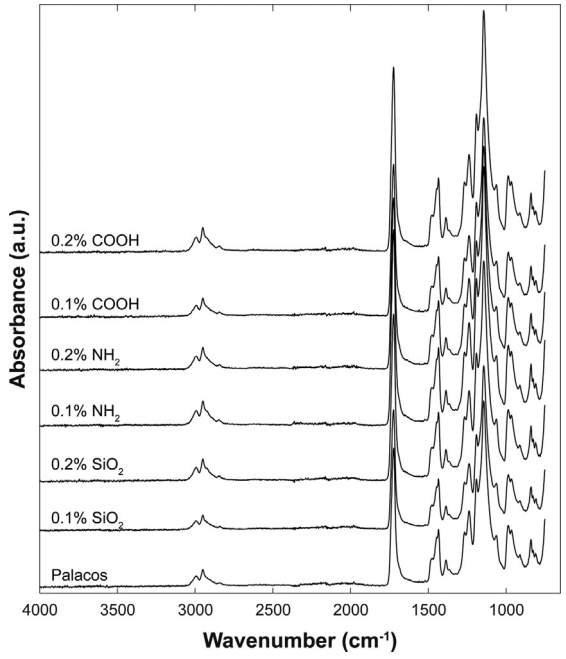

Fig. 6 – ATR-FTIR spectra collected for each cement.

peaks occurred at 1730 cm^{-1} and 1140 cm^{-1} which correspond to a C=O stretch and O–C–C stretch, respectively. Analysis of ATR-FTIR spectra showed no differences in the position of intensity peaks between the different cements, indicating that there was no formation of new chemical groups. However, peak intensities did increase with the addition of MSNs except for 0.1% SiO_2.

3.2.4. *Thermal characteristics*

The initial decomposition temperature of the cements was found to decrease with the addition of MSNs and surface functionalization increased this negative effect (Table 5).

Table 5 – The initial thermal decomposition temperature (T_{10}), midpoint decomposition (T_{50}), and glass transition (T_g) obtained from TGA and DSC testing.

Sample	T_{10} (°C)	T_{50} (°C)	T_g (°C)
Palacos	340.11	384.08	99.69
0.1% SiO_2	336.20	381.43	100.44
0.2% SiO_2	326.09	380.79	99.29
0.1% NH_2	323.96	380.73	102.30
0.2% NH_2	325.02	381.59	100.85
0.1% COOH	323.22	381.76	100.29
0.2% COOH	320.70	379.94	99.39

Midpoint decomposition temperatures tended to equalize between all cements. This is potentially attributable to degradation of functional groups on the MSN surface. The glass transition temperature was not influenced by the addition of MSNs.

4. Discussion

In this study, we extend upon our previous work with nanoparticle-reinforced bone cement (Slane et al., 2014) in an effort to enhance particle dispersion and interfacial adhesion using low loadings of functionalized MSNs. Two functional groups (and plain MSNs as a positive control) at loading ratios of 0.1% and 0.2% wt/wt were incorporated into a commercially available acrylic bone cement. The functional groups used, propylamine and propylcarboxylic acid, were chosen based upon previous research on bone cement modified with functionalized carbon nanotubes (Ormsby et al., 2010b). Mixed results were observed for the mechanical properties of the cements. Four-point flexural testing and nanoindentation revealed minimal impact on the properties of the cements, except for several changes in the nano-level

mechanical properties. Conversely, microindentation testing demonstrated that the addition of MSNs significantly altered the properties of the cements. This finding suggests the presence of different reinforcement mechanisms, which will be addressed in greater depth later in the discussion. To the authors' current knowledge, this is the first study to utilize a multiscale approach to characterize the influence of nanoparticle reinforcement on acrylic bone cement.

The concept of adding reinforcement materials to enhance the mechanical properties of acrylic bone cement is not novel; in the mid 1970s researchers experimented with bone cements modified with graphite and carbon fibers (Knoell et al., 1975; Pilliar et al., 1976). Despite the long history associated with reinforced bone cements, a variety of problems persist which limit their clinical applicability such as poor material dispersion, poor fiber/particle interfacial adhesion with the cement matrix and diminished mixing characteristics. Regardless of the chosen reinforcement material, one of the primary difficulties faced with polymer composites is achieving a uniform dispersion of the reinforcement. If this is not achieved, the agglomerations of fibers/particles can form stress concentration sites within the polymer matrix leading to premature failure with the application of load (Ormsby et al., 2010a). Surface functionalization, a process where chemical moieties are covalently linked to a particle/fibers surface, is a widely implemented technique that can assist in particle dispersion and interfacial adhesion (Ma et al., 2010). Previous work with bone cement demonstrated that functionalized carbon nanotubes could enhance several different mechanical properties (Ormsby et al., 2010b).

Mesoporous silica nanoparticles have been shown to enhance the mechanical properties of polymer composites. Samuel et al. modified a dental resin with MSNs and found an increase in the flexural modulus and no effect on the flexural strength with increasing MSN content(Samuel et al., 2009) while Ji et al. demonstrated drastic improvements in the tensile properties of a polymer composite loaded with MSNs (Ji et al., 2003). Similarly, Park and Pinnavaia showed enhanced tensile properties and toughness with an epoxy resin modified with mesoporous silica foam particles (Park and Pinnavaia, 2007). However, all of these studies used loading ratios considerably higher than in the current study. Our previous work on MSN-modified bone cements used loading ratios of 0.5%, 2%, and 5% wt/wt. While several encouraging results were found, we wanted to determine if low-loading ratios could enhance the properties of cement while minimizing the impact on the handling characteristics. In theory, the high surface area of the MSNs used in this study (720 m^2/g) suggest an efficient stress transfer mechanism between the particle and polymer matrix can develop (Fu et al., 2008).

The flexural properties measured in this study are in close agreement with previously published values. For example, Dunne reported a flexural strength and modulus for Palacos R (cured in air for 24 h) of 75.67 MPa and 2.76 GPa, respectively (Dunne, 2008), compared to 72.07 MPa and 2.81 GPa in this study. The flexural strength and modulus of the cements were not influenced by the addition of MSNs and all cements displayed properties above those outlined in ISO 5833. This is likely attributable to the low loadings used, which were insufficient to induce changes on the macro level. SEM analysis of the fracture surfaces of bending samples also displayed no apparent differences, indicating that the failure mechanism was consistent across all groups. Several previous studies have examined the use of nanomaterials to reinforce acrylic bone cement, however, the results are somewhat conflicting. For example, Ormsby et al. incorporated various loadings of functionalized carbon nanotubes (f-CNTs) into Colacryl bone cement. They found a 4.1% decrease in the flexural strength using 0.1 wt/wt propylamine CNTs and a 21.9% increase using 0.1 wt/wt propylcarboxylic acid CNTs (Ormsby et al., 2010b). In contrast, Gonçalves et al. observed an ~25% decrease in the flexural strength of an acrylic cement modified with 0.1 wt/wt f-CNTs, which they attributed to the CNTs acting as free-radical scavengers, resulting in polymerization retardation and inhibition (Gonçalves et al., 2012). Based on the glass transition temperatures determined in this study, which were consistent across all groups, we do not believe that the MSNs inhibited the polymerization of the cement.

Nanoindentation testing revealed only slight differences in measures of hardness and modulus with only several significant variations detected. In contrast, microindentation showed that the inclusion of MSNs significantly enhanced the hardness of all cements. This finding highlights the differences between micro and nanoindentation. The indentation data collected generally agrees with that previously published for bone cement. Karimzadeh and Ayatollahi performed nanoindentation testing on Cemex RX cement and found a modulus of 5.56 GPa and hardness of 290 MPa (Karimzadeh and Ayatollahi, 2012). These values are slightly higher than those found in this study, however, they used a peak indentation depth of 210 nm which is substantially smaller than that used in this study, and due to the indentation size effect the measured properties are expected to be higher. Lewis et al. obtained samples of Palacos R from retrieved cement mantles and found a modulus of 3.78 GPa and hardness of 169 MPa for cement that was implanted for 11 months using nanoindentation (Lewis et al., 2006). Lelovics and Liptakova performed microindentation on SmartSet cement and found a microhardness of 199 MPa (Lelovics and Liptakova, 2010), which generally agrees with the value of 172 MPa determined in this study.

Compared to the size of the particles used in this study (200 nm), nanoindentation and microindentation can probe different heterogeneities within the cement since the local mechanical properties are directly linked to the size of the contact. The relative size of the indentation surface/volume varies substantially between the two techniques with nanoindentation being hundreds of nanometers (~750 nm depth, <5 μm diagonal) and microindentation hundreds of microns (~300–400 μm diagonal). The hardness of a material represents its ability to resist surface deformation to an applied load. In a material such as PMMA, non-recoverable deformation of the surface possibly results from rupture of the localized polymer matrix network at the site of load application or slippage between the matrix and any present reinforcement material (Shen et al., 2006). At the micro level, substantially more MSNs are within the indented cement volume, thus leading to an increase in the measured

hardness. For 0.1% MSN loadings, it was found that functionalization significantly increased microhardness, however, this is likely due to enhanced dispersion and not the result of new bond formation between the particle and matrix (as confirmed with ATR-FTIR). Additionally, hardness measured with nanoindentation was typically higher than the calculated microhardness. This finding is due to differences in how contact area is measured between the techniques (Qian et al., 2005) and the confined polymer mobility of the interfacial region adjacent to the indenter tip (Tehrani et al., 2011).

Particle dispersion within the cement matrix was significantly influenced by particle surface functionalization. As verified with SEM (Figs. 3 and 4), SiO_2 particles tended to form large agglomerates often times with interfacial gaps between the particle and the matrix. In contrast, functionalized particles were more evenly dispersed throughout the matrix. Agglomerations still occurred with functionalized particles, however, they generally were less frequent and smaller in size. It appears that the sonication process used to disperse MSNs was adequate for functionalized particles but not for SiO_2. While ultrasonication is a powerful tool to disrupt particle agglomerations, care must be taken since in some situations (e.g. extended sonication times) the applied acoustic energy can actually induce the formation of new agglomerates or damage the particle/fiber being dispersed (such as carbon nanotube scission) (Taurozzi et al., 2011).

Bone cement acts as a grouting material between the implant and the patient's bone, providing immediate implant fixation while distributing forces from the implant to the surrounding bone bed. Therefore, it must possess properties that are the intermediately of the prosthesis (typically titanium or cobalt chrome) and bone. Dynamic mechanical analysis conducted in this study confirms that this is the case for all cements tested. At a frequency of 1 Hz and strain of 0.01%, the storage modulus of cements ranged from 3.1 to 3.4 GPa while tan δ varied between 0.07 and 0.08. In contrast, cancellous bone has a storage modulus of 0.2 GPa and tan δ of 0.09–0.1 (cortical bone 0.04) while metals used for implants typically have a storage modulus of exceeding 100 GPa and a tan δ of 10^{-4} (De Santis et al., 2003). It was found that the addition of MSNs had minimal impact on the viscoelastic properties of the cements and generally, values for storage modulus and tan δ were consistent. Interestingly, at a frequency of 40 Hz tan δ values significantly increased. This is in marked contrast to skeletal tissue where tan δ decreases with increasing loading frequency, indicating the material acts as an elastic solid and transmits rather than dissipates force. It has been suggested that this increase in tan δ with higher frequencies enable acrylic cements to survive the loading patterns they are exposed to during gait, despite the fact that cements fail in a brittle fashion during static testing (Daniels et al., 2005).

Several limitations of the current study are acknowledged. Firstly, only a single type of mesoporous silica with a specific size and structure was used. A variety of MSNs can be fabricated with different pores sizes, surface areas, and pore volumes. These factors could potentially influence the findings from this study. One exceptionally attractive alternative is mesoporous silica foam, which has a very large pore volume (e.g. 2.4 cm^3/g) and an open structure that could allow for strong bonding with polymer chains (Park and Pinnavaia, 2007). Secondly, only a single variety of acrylic bone cement was used although many other formulations exist. Different cements with alternative chemical compositions and viscosities may respond differently to the inclusion of MSNs. As mentioned previously, the cement used in this study was chosen since it is one of the most widely used in the North American and European markets. Thirdly, only a single type of static testing was conducted. Other methods commonly used to test bone cement such as tension and compression could potentially demonstrate enhancements, or detrimental, effects on the properties of the cement. Four-point bending was used since it includes both tensile and compression components and is thought to be a realistic testing method for bone cement (Kuehn et al., 2005). Fourthly, micro and nanoindentation testing were performed on different samples, although samples were prepared at the same time from the same batch of cement. The observed differences in micro and nanoindentation findings could potentially result from sample inhomogeneity. Finally, fatigue testing of the cements was not performed, although it is well known that mechanical failure of bone cement can result from fatigue failure (Lewis, 2003). It was deemed beyond the scope of this project to conduct fatigue testing.

Despite these limitations, this is the first study (to the authors' current knowledge) that has utilized a multiscale approach to characterize the mechanical properties of nanoparticle-reinforced bone cement. Contrary to our previous work with MSN-modified cements, in this study the addition of mesoporous silica did not have a detrimental influence on the properties of the cements. Future work should include examining alternative functionalization groups that can create the formation of interfacial bonds between the particle and PMMA matrix. One potential method would be to alter the hydrophilicity of the particle's surface since it has previously been demonstrated that hydrophobic mesoporous silica can aid in dispersion and increase adhesion (Bento et al., 2013). Higher loading ratios of MSNs should be considered, however, with increased loading the potential for diminished handling characteristics and altered polymerization characteristics increase. Therefore, it would be required to quantify the influence of higher MSNs loadings on the rheological behavior and setting polymerization behavior of the cement. Finally, one potential benefit of MSN-modified cement not explored in this study is the ability of MSNs to reduce volumetric shrinkage during polymerization (Samuel et al., 2009), which can be as high as 6–7%. It is known that the shrinkage of bone cement can induce residual stresses as high as 10 MPa in the cement, potentially causing cracks that would act as failure initiation sites (Roques et al., 2004).

5. Conclusion

In this study, a commercially available acrylic bone cement was modified with low-loadings of functionalized mesoporous silica nanoparticles and the resulting impact on the cement's mechanical and material properties were quantified over different length scales. Results from this study indicate

that the loading ratios of MSNs used were insufficient to influence the macro level properties of the cement. Functionalization aided in particle dispersion but did not appear to result in enhanced interfacial adhesion between the particle and the matrix. These results suggest that that loading ratios of mesoporous silica used are not an effective reinforcement material in acrylic bone cement. Additionally, since non-functionalized MSNs were found to form large agglomerates, their use in bone cement is not recommended regardless of the loading ratio. Future work should be conducted to determine the impact of higher MSN loading ratios and alternative functional groups.

Acknowledgments

The authors thank Christopher Besaw for his work on the microindentation testing. The authors gratefully acknowledge use of facilities and instrumentation supported by the NSF-funded University of Wisconsin Materials Research Science and Engineering Center (DMR-1121288).

REFERENCES

Adelani, M.A., Keeney, J.A., Palisch, A., Fowler, S.A., Clohisy, J.C., 2013. Has total hip arthroplasty in patients 30 years or younger improved? A systematic review. Clin. Orthop Relat. Res. 471, 2595–2601.

Ania, F., Broza, G., Mina, M.F., Schulte, K., Roslaniec, Z., Baltá-Calleja, F.J., 2006. Micromechanical properties of poly(butylene terephthalate) nanocomposites with single- and multi-walled carbon nanotubes. Compos. Interface 13, 33–45.

Arun, S., Rama Sreekanth, P.S., Kanagaraj, S., 2014. Mechanical characterisation of PMMA/SWNTs bone cement using nanoindenter. Mater. Technol. 29, B4–B9.

ASTM International, 2012. Standard Test Method for Transition Temperatures and Enthalpies of Fusion and Crystallization of Polymers by Differential Scanning Calorimetry. ASTM International West Conshohocken, PA.

Ayatollahi, M., Karimzadeh, A., 2012. Determination of fracture toughness of bone cement by nano-indentation test. Int. J. Fract. 175, 193–198.

Beake, B.D., Chen, S., Hull, J.B., Gao, F., 2002. Nanoindentation behavior of clay/poly(ethylene oxide) nanocomposites. J. Nanosci. Nanotechnol. 2, 73–79.

Bento, A., Lourenço, J.P., Fernandes, A., Cerrada, M.L., Rosário Ribeiro, M., 2013. Functionalization of mesoporous MCM-41 (nano)particles: preparation methodologies, role on catalytic features, and dispersion within polyethylene nanocomposites. ChemCatChem 5, 966–976.

Chaplin, R.P., Lee, A.J., Hooper, R.M., Clarke, M., 2006. The mechanical properties of recovered PMMA bone cement: a preliminary study. J. Mater. Sci. Mater. Med. 17, 1433–1448.

Chung, S.M., Yap, A.U., Tsai, K.T., Yap, F.L., 2005. Elastic modulus of resin-based dental restorative materials: a microindentation approach. J. Biomed. Mater. Res. B Appl. Biomater. 72, 246–253.

Daniels, A., Wirz, D., Morscher, E., 2005. Properties of bone cement: extreme differences in properties of successful bone cements. In: Breusch, S., Malchau, H. (Eds.), The Well-Cemented Total Hip Arthroplasty. Springer, Berlin.

De Santis, R., Mollica, F., Ambrosio, L., Nicolais, L., Ronca, D., 2003. Dynamic mechanical behavior of PMMA based bone cements in wet environment. J. Mater. Sci. Mater. Med. 14, 583–594.

Dhakal, H.N., Zhang, Z.Y., Richardson, M.O.W., 2006. Nanoindentation behaviour of layered silicate reinforced unsaturated polyester nanocomposites. Polym. Test. 25, 846–852.

Dunne, N., 2008. Mechanical properties of bone cement. In: Deb, S. (Ed.), Orthopaedic Bone Cements. Woodhead Publishing Limited, Cambridge, pp. 233–264.

Fischer-Cripps, A., 2011. In: Nanoindentation. Springer, Dordrecht.

Fu, S., Feng, X., Lauke, B., Mai, Y., 2008. Effects of particle size, particle/matrix interface adhesion and particle loading on mechanical properties of particulate–polymer composites. Compos. Part B-Eng. 39, 933–961.

Gonçalves, G., Cruz, S.M., Ramalho, A., Grácio, J., Marques, P.A., 2012. Graphene oxide versus functionalized carbon nanotubes as a reinforcing agent in a PMMA/HA bone cement. Nanoscale 4, 2937–2945.

Guo, Z., Pereira, T., Choi, O., Wang, Y., Hahn, H.T., 2006. Surface functionalized alumina nanoparticle filled polymeric nanocomposites with enhanced mechanical properties. J. Mater. Chem. 16, 2800–2808.

Hailer, Garellick, N.P., Karrholm, J., G., 2010. Uncemented and cemented primary total hip arthroplasty in the Swedish Hip Arthroplasty Register. Acta Orthop. 81, 34–41.

International Organization for Standardization, 2002. Implants for Surgery – Acrylic Resin Cements. ISO, Geneva, Switzerland.

Izquierdo-Barba, I., Colilla, M., Vallet-Regi, M., 2008. Nanostructured mesoporous silicas for bone tissue regeneration. J. Nanomater, 1–14.

Jayasuriya, R.L., Buckley, S.C., Hamer, A.J., Kerry, R.M., Stockley, I., Tomouk, M.W., Wilkinson, J.M., 2013. Effect of sliding-taper compared with composite-beam cemented femoral prosthesis loading regime on proximal femoral bone remodeling: a randomized clinical trial. J. Bone Joint Surg. Am. 95, 19–27.

Jeffers, J.R., Browne, M., Lennon, A.B., Prendergast, P.J., Taylor, M., 2007. Cement mantle fatigue failure in total hip replacement: experimental and computational testing. J. Biomech. 40, 1525–1533.

Ji, X., Hampsey, J.E., Hu, Q., He, J., Yang, Z., Lu, Y., 2003. Mesoporous silica-reinforced polymer nanocomposites. Chem. Mater. 15, 3656–3662.

Kane, R.J., Yue, W., Mason, J.J., Roeder, R.K., 2010. Improved fatigue life of acrylic bone cements reinforced with zirconia fibers. J. Mech. Behav. Biomed. 3, 504–511.

Karimzadeh, A., Ayatollahi, M.R., 2012. Investigation of mechanical and tribological properties of bone cement by nano-indentation and nano-scratch experiments. Polym. Test. 31, 828–833.

Khaled, S.M., Charpentier, P.A., Rizkalla, A.S., 2011. Physical and mechanical properties of PMMA bone cement reinforced with nano-sized titania fibers. J. Biomater. Appl. 25, 515–537.

Khanuja, H.S., Vakil, J.J., Goddard, M.S., Mont, M.A., 2011. Cementless femoral fixation in total hip arthroplasty. J. Bone Joint Surg. Am. 93, 500–509.

Knoell, A., Maxwell, H., Bechtol, C., 1975. Graphite fiber reinforced bone cement. An experimental feasibility investigation. Ann. Biomed. Eng. 3, 225–229.

Kordás, K., Kukkola, J., Tóth, G., Jantunen, H., Szabó, M., Sápi, A., Kukovecz, A., Kónya, Z., Mikkola, J., 2013. Nanoparticle dispersions. In: Vajtai, R. (Ed.), Springer Handbook of Nanomaterials. Springer-Verlag, Berlin, pp. 729–775.

Kuehn, K.D., Ege, W., Gopp, U., 2005. Acrylic bone cements: mechanical and physical properties. Orthop. Clin. N. Am. 36, 29–39 (v–vi).

Kumar, B., Cooke, F.W., 2006. Fatigue behaviour of fiber reinforced bone cement. In: Gdoutos, E.E. (Ed.), Fracture of Nano and Engineering Materials and Structures. Springer, Netherlands, pp. 1023–1024.

Lach, R., Kim, G.-M., Michler, G.H., Grellmann, W., Albrecht, K., 2006. Indentation fracture mechanics for toughness assessment of PMMA/SiO_2 nanocomposites. Macromol. Mater. Eng. 291, 263–271.
Lelovics, H., Liptakova, T., 2010. Time and mixing technique-dependent changes in bone cement SmartSet(R) HV. Acta Bioeng. Biomech./Wroclaw Univ. Technol. 12, 63–67.
Lennon, A.B., 2008. Fracture toughness and fatigue characteristics of bone cements. In: Deb, S. (Ed.), Orthopaedic Bone Cements. Woodhead Publishing Limited, Cambridge, pp. 265–310.
Lewis, G., 2003. Fatigue testing and performance of acrylic bone-cement materials: state-of-the-art review. J. Biomed. Mater. Res. B Appl. Biomater. 66, 457–486.
Lewis, G., Janna, S., 2003. Effect of test specimen cross-sectional shape on the in vitro fatigue life of acrylic bone cement. Biomaterials 24, 4315–4321.
Lewis, G., Xu, J., Dunne, N., Daly, C., Orr, J., 2006. Critical comparison of two methods for the determination of nanomechanical properties of a material: application to synthetic and natural biomaterials. J. Biomed. Mater. Res. Part B, Appl. Biomater. 78, 312–317.
Ma, P.-C., Siddiqui, N.A., Marom, G., Kim, J.-K., 2010. Dispersion and functionalization of carbon nanotubes for polymer-based nanocomposites: a review. Compos. Part A – Appl. Sci. 41, 1345–1367.
Malzbender, J., Steinbrech, R.W., 2004. Mechanical properties of coated materials and multi-layered composites determined using bending methods. Surf. Coat. Technol. 176, 165–172.
Marrs, B., Andrews, R., Rantell, T., Pienkowski, D., 2006. Augmentation of acrylic bone cement with multiwall carbon nanotubes. J. Biomed. Mater. Res. Part A 77, 269–276.
Musib, M., Jones, J., Chakote, K., Hayes, W., Saha, S., 2012. Microhardness of bi-antibiotic-eluting bone cement scaffolds. Prog. Biomater. 1, 1–7.
Nottrott, M., Molster, A.O., Gjerdet, N.R., 2007. Time dependent mechanical properties of bone cement. An in vitro study over one year. J. Biomed. Mater. Res. B Appl. Biomater. 83, 416–421.
O'Connor, D.O., Burke, D.W., Jasty, M., Sedlacek, R.C., Harris, W.H., 1996. In vitro measurement of strain in the bone cement surrounding the femoral component of total hip replacements during simulated gait and stair-climbing. J. Orthop. Res.: Off. Publ. Orthop. Res. Soc. 14, 769–777.
Oliver, W.C., Pharr, G.M., 2004. Measurement of hardness and elastic modulus by instrumented indentation: advances in understanding and refinements to methodology. J. Mater. Res. 19, 3–20.
Ormsby, R., McNally, T., Mitchell, C., Dunne, N., 2010a. Incorporation of multiwalled carbon nanotubes to acrylic based bone cements: effects on mechanical and thermal properties. J. Mech. Behav. Biomed. 3, 136–145.
Ormsby, R., McNally, T., Mitchell, C., Dunne, N., 2010b. Influence of multiwall carbon nanotube functionality and loading on mechanical properties of PMMA/MWCNT bone cements. J. Mater. Sci. Mater. Med. 21, 2287–2292.
Ormsby, R., McNally, T., O'Hare, P., Burke, G., Mitchell, C., Dunne, N., 2012. Fatigue and biocompatibility properties of a poly (methyl methacrylate) bone cement with multi-walled carbon nanotubes. Acta Biomater. 8, 1169–1179.
Padmanabhan, S.K., Balakrishnan, A., Chu, M.C., Kim, T.N., Cho, S.J., 2010. Micro-indentation fracture behavior of human enamel. Dent. Mater. 26, 100–104.
Park, I., Pinnavaia, T.J., 2007. Mesocellular silica foam as an epoxy polymer reinforcing agent. Adv. Funct. Mater. 17, 2835–2841.
Park, S., Hung, C.T., Ateshian, G.A., 2004. Mechanical response of bovine articular cartilage under dynamic unconfined compression loading at physiological stress levels. Osteoarthr. Cartil. 12, 65–73.
Pegel, S., Pötschke, P., Petzold, G., Alig, I., Dudkin, S.M., Lellinger, D., 2008. Dispersion, agglomeration, and network formation of multiwalled carbon nanotubes in polycarbonate melts. Polymer 49, 974–984.
Pilliar, R.M., Blackwell, R., Macnab, I., Cameron, H.U., 1976. Carbon fiber-reinforced bone cement in orthopedic surgery. J. Biomed. Mater. Res. B Appl. Biomater. 10, 893–906.
Qian, L., Li, M., Zhou, Z., Yang, H., Shi, X., 2005. Comparison of nano-indentation hardness to microhardness. Surf. Coat. Technol. 195, 264–271.
Roques, A., Browne, M., Taylor, A., New, A., Baker, D., 2004. Quantitative measurement of the stresses induced during polymerisation of bone cement. Biomaterials 25, 4415–4424.
Samuel, S.P., Li, S., Mukherjee, I., Guo, Y., Patel, A.C., Baran, G., Wei, Y., 2009. Mechanical properties of experimental dental composites containing a combination of mesoporous and nonporous spherical silica as fillers. Dent. Mater. 25, 296–301.
Schiffmann, K.I., 2006. Nanoindentation creep and stress relaxation tests of polycarbonate: analysis of viscoelastic properties by different rheological models. Int. J. Mater. Res. 97, 1199–1211.
Shen, L., Wang, L., Liu, T., He, C., 2006. Nanoindentation and morphological studies of epoxy nanocomposites. Macromol. Mater. Eng. 291, 1358–1366.
Slane, J., Vivanco, J., Meyer, J., Ploeg, H.L., Squire, M., 2014. Modification of acrylic bone cement with mesoporous silica nanoparticles: effects on mechanical, fatigue and absorption properties. J. Mech. Behav. Biomed. Mater. 29, 451–461.
Sonntag, R., Reinders, J., Kretzer, J.P., 2012. What's next? Alternative materials for articulation in total joint replacement. Acta Biomater. 8, 2434–2441.
Taurozzi, J.S., Hackley, V.A., Wiesner, M.R., 2011. Ultrasonic dispersion of nanoparticles for environmental, health and safety assessment – issues and recommendations. Nanotoxicology 5, 711–729.
Tehrani, M., Safdari, M., Al-Haik, M.S., 2011. Nanocharacterization of creep behavior of multiwall carbon nanotubes/epoxy nanocomposite. Int. J. Plast. 27, 887–901.
Xu, H.H.K., Quinn, J.B., Smith, D.T., Antonucci, J.M., Schumacher, G.E., Eichmiller, F.C., 2002. Dental resin composites containing silica-fused whiskers – effects of whisker-to-silica ratio on fracture toughness and indentation properties. Biomaterials 23, 735–742.
Zhang, F.-A., Lee, D.-K., Pinnavaia, T.J., 2010. PMMA/mesoporous silica nanocomposites: effect of framework structure and pore size on thermomechanical properties. Polym. Chem. 1, 107–113.